International Journal of Pharmaceutics 429 (2012) 104–112

Contents lists available at SciVerse ScienceDirect

International Journal of Pharmaceutics

journal homepage: www.elsevier.com/locate/ijpharm

Pharmaceutical Nanotechnology

Self nanoprecipitating preconcentrate of tamoxifen citrate for enhanced bioavailability

Sonali V. Kapse[a], Rajiv V. Gaikwad[b], Abdul Samad[b], Padma V. Devarajan[a,*]

[a] Department of Pharmaceutical Sciences and Technology, Institute of Chemical Technology, Matunga, Mumbai 400 019, India
[b] Veterinary Nuclear Medicine Center, Department of Medicine, Bombay Veterinary College, Parel, Mumbai 400 012, India

ARTICLE INFO

Article history:
Received 15 December 2011
Received in revised form 23 February 2012
Accepted 26 February 2012
Available online 5 March 2012

Keywords:
Self nanoprecipitating preconcentrate
Tamoxifen citrate
Polymeric nanoparticles
In situ nanoprecipitation
Bioavailability
Scintigraphy

ABSTRACT

We disclose a self nanoprecipitating preconcentrate (SNP) of tamoxifen citrate (TMX), which forms TMX loaded polymeric nanoparticles, on dilution with aqueous media. SNP comprised TMX, polymer (Kollidon SR) and surfactant/s dissolved in a pharmaceutically acceptable vehicle. Binary surfactant mixtures of Aerosol OT (AOT) with Tween 80 revealed synergistic reduction in surface tension to enable both high entrapment efficiency (EE) and low particle size (PS). Synergism of the surfactants was confirmed by molecular interaction parameter(β^{σ}). Combination of AOT and Tween 80 resulted in EE (~85%) and PS (<250 nm). Formation of TMX-KSR nanoparticles in situ was reproducible under most experimental conditions and exhibited pH independent behavior. Dilution volume (>80 mL) influenced both PS and EE while dilution temperature influenced only PS. Marginal increase in size was evident at the end of 1 h nevertheless was not of concern as TMX SNP exhibited near complete release in 1 h. DSC and XRD studies revealed amorphous nature of TMX in nanoparticles. FTIR imaging confirmed uniform distribution of TMX in nanoparticles. ESEM and TEM revealed spherical nanoparticles. Biodistribution studies of ^{99m}Tc labeled TMX SNP in rats revealed no significant absorption however oral pharmacokinetics revealed enhanced oral bioavailability of TMX (165%) compared to TMX suspension. SNP presents a new in situ approach, for design of drug loaded polymeric nanoparticles.

© 2012 Elsevier B.V. All rights reserved.

1. Introduction

Polymeric nanoparticles as drug delivery systems (DDS) have been extensively investigated for manifold applications. Bioenhancement of poorly water soluble drugs using nanotechnology approaches has been recently reviewed (Fasinu et al., 2011). Polymeric nanoparticles enable controlled release of drugs, protection of labile drugs especially peptides, proteins, nucleic acids and serve as carriers for targeted and intracellular drug delivery (Jain, 2000; Soppimath et al., 2001; Chawla and Amiji, 2002; Panyam and Labhasetwar, 2003; Allen and Cullis, 2004; Couvreur and Vauthier, 2006; Farokhzad et al., 2006).

TMX is recommended for long-term prophylactic therapy in high-risk and post-menopausal women and in advanced or metastatic breast cancer treatment (Buckley and Goa, 1989). TMX exhibits low oral bioavailability, large interindividual variations and extensive liver metabolism, often necessitating high dose with resultant side effects (McVie et al., 1986; Tukker et al., 1986). The therapeutic advantage of oral nanoparticles of TMX is recently reported (Jain et al., 2011).

Technological hurdles that hamper scale-up of polymeric nanoparticles present a major constraint in their exploitation for drug delivery. Simple and practical approaches that address the above are therefore imperative. Nevertheless, achieving high entrapment efficiency and nanosize could prove rate limiting.

Bodmeier et al. have discussed the generation of microparticles in situ for a number of drugs including leuprolide acetate (Dong et al., 2006; Luan and Bodmeier, 2006a, 2006b) lysozyme (Körber and Bodmeier, 2008), vinpocetine (Li et al., 2008), diltiazem hydrochloride (Kranz and Bodmeier, 2007), buserelin acetate (Kranz et al., 2001; Kranz and Bodmeier, 2007) and bupivacaine hydrochloride (Kranz et al., 2001; Kranz and Bodmeier, 2007). A two-syringe/connector system comprising one syringe (single syringe) containing a solution of drug and polymer (internal phase) and another syringe containing oil/aqueous media (external phase) were mixed using connector system to form an o/o emulsion. This emulsion when injected into the body fluids formed microparticles in situ (Luan and Bodmeier, 2006a).

We present in this study a simple method for generation of drug loaded polymeric nanoparticles in situ. The system discussed in the study is a self nanoprecipitating preconcentrate (SNP), a monophasic liquid composed of drug, polymer (Kollidon SR) and surfactants which on aqueous dilution could reproducibly provide drug loaded TMX nanoparticles. The objective of the present study was

* Corresponding author at: Tel.: +91 22 33612201; fax: +91 22 3361 1020.
E-mail address: pvdevarajan@gmail.com (P.V. Devarajan).

0378-5173/$ – see front matter © 2012 Elsevier B.V. All rights reserved.
doi:10.1016/j.ijpharm.2012.02.042

development and optimization of an SNP of TMX to obtain high drug entrapment and nanosize to enhance bioavailability.

2. Materials and methods

2.1. Materials

tamoxifen citrate (TMX) was kindly provided by Ar-Ex. Laboratories Pvt. Ltd. (India), Transcutol-P (diethylene glycol monoethyl ether) and Labrasol by Gattefosse (India), Kollidon SR (KSR), Pluronic F68 (PF-68) and Solutol HS 15 by BASF (India), and Myrj-52 by Uniquema (India). Aerosol OT (sodium bis(2-ethylhexyl) sulfosuccinate) [AOT], propylene glycol, PEG 400, glycerol and Tween 80 (polyoxyethylene 20 sorbitan monooleate) were purchased from S.D. Fine Chemicals (India).

2.2. Solubility studies

Equilibrium solubility of TMX and solubility of KSR were determined in various solubilizer/s namely Olivem 300, Solutol HS-15, Labrasol, Myrj-52, Tween 80, Transcutol-P, propylene glycol, PEG 400 and glycerol. Briefly, excess TMX was added to 1 mL of each solubilizer in eppendorf tubes. The tubes were sealed and vortex mixed intermittently followed by sonication and equilibration at room temperature for 24 h. Equilibrated samples were centrifuged at 15,000 rpm for 15 min, and the supernatant was analyzed for TMX by UV spectrophotometry at λ_{max} 275 nm. Approximate solubility of KSR was determined by incremental addition of 5 mg polymer, to glass test tubes containing 1 mL solubilizer, followed by vortex mixing and sonication, till no more polymer dissolved. Each study was performed in triplicate.

2.3. Formulation of SNP

SNP was prepared by simple solution of TMX (15.2 mg/mL), polymer (KSR) and surfactants in Transcutol-P as vehicle. An anionic surfactant AOT (w/v) and the non-ionic surfactants Tween 80 (v/v), Myrj-52 (v/v) and PF-68 (w/v) were evaluated. The type and concentration of surfactant and the polymer concentration were varied to obtain SNPs that could generate dispersions of nanosize with high EE.

2.4. Evaluation of SNP

2.4.1. Viscosity

Viscosity of SNP was determined by capillary tube viscometer (Oswald viscometer) at 25 °C using water as the reference (viscosity of water = 0.008 cP). Each measurement was recorded in triplicate.

2.4.2. Surface tension

Surface tension of SNP was determined by drop number method at 25 °C from a height of 5 cm. Measurements were performed using water as the reference (surface tension of water = 72 dyne/cm). Each measurement was recorded in triplicate.

2.5. Evaluation of SNP for formation of polymeric nanoparticles in situ

SNP was evaluated for spontaneous formation of drug loaded polymeric nanoparticles in situ by gradual addition of 1 mL of the SNP to aqueous medium under magnetic stirring. The nanodispersions obtained were evaluated for the following.

2.5.1. Entrapment efficiency (EE)

EE was determined by separating the nanoparticles from dispersion by centrifugation (Eltek 4100 D Research Centrifuge) at 15,000 rpm for 30 min. The supernatant obtained after centrifugation was suitably diluted and analyzed for free TMX by UV spectrophotometry (Shimadzu, Japan) at λ_{max} 275 nm.

2.5.2. Particle size (PS)

Particle size was determined by photon correlation spectroscopy using the N4 Plus Submicron Particle Size Analyzer (Beckman Coulter™) at 25 °C. All the measurements were taken by scattering light at 90°. Particle size was determined by diluting the nanoparticle dispersion with water to obtain final counts per second (intensity), 5×10^4 to 1×10^6. The water used for dilution was filtered through 0.22 μm membrane filter.

2.5.3. Zeta potential (ξ)

Zeta potential measurements were performed on the Delsa™ Nano-C (Beckman Coulter®, USA) to assess surface charge and stability of the nanodispersion. Zeta potential was determined by introducing the nanodispersion into the electrophoretic capillary type cell with applied electric field of −15.79 V/cm. All measurements were recorded in triplicate.

SNP performance was evaluated by diluting the SNP with different aqueous media. pH 1.2 HCl, pH 2.5, pH 6.8 and pH 7.4 varying from 4 mL to 200 mL and simulated gastric fluid (SGF) 40 mL prepared as per Indian Pharmacopeia 1996 were evaluated. Effect of time (5, 15, 30 and 60 min) and temperature (15 °C, 28 °C and 50 °C) on EE and PS were evaluated.

The nanodispersion was centrifuged and the nanoparticle pellet separated, air dried and characterized for DSC, XRD, FTIR and FTIR microscopy.

2.5.4. Differential scanning calorimetry (DSC)

The dried nanoparticle sample was accurately weighed (5 mg) in aluminum pans, sealed and subjected to DSC on Perkin Elmer Pyris 6 DSC thermal analysis instrument. Thermograms were recorded by heating samples from 35 °C to 350 °C at a heating rate of 10 °C/min under nitrogen flow using an empty aluminum pan as the reference.

2.5.5. X-ray diffraction (XRD)

XRD patterns of dried nanoparticle samples were recorded at room temperature on a Philips Pro Analytical Xpert PRO MPD diffractometer with nickel filtered Cu Kα radiation operated at a voltage of 3 kV, 5 mA current, 4°/min scanning speed, and 5–60° (2θ) range.

2.5.6. Fourier transform infrared spectroscopy (FTIR)

FTIR spectra were recorded in the range of 450–4500 cm^{-1} on a Perkin Elmer FTIR Spectrometer Spectrum RXI. Dried nanoparticles were mulled with anhydrous potassium bromide, compressed to form a thin transparent pellet and subjected to FTIR.

2.5.7. Fourier transform infrared spectroscopy (FTIR) microscopy and imaging

FTIR microscopy and imaging were performed on a Spotlight 100 FTIR with Spotlight 300 Microscope and MCT detector. Microscopy imaging was performed in the range of 4000–720 cm^{-1} with image point size (25 μm × 25 μm) at interval of 8 cm^{-1} with resolution of 16 cm^{-1} and scan/pixel of 2. Dried nanoparticles were dispersed in mineral oil for imaging.

2.5.8. Environmental scanning electron microscopy (ESEM)

Nanoparticle sample for ESEM was prepared by dispersing the isolated pellet in 5 mL water. A drop of this dispersion was deposited on an aluminum grid and imaging was performed on a FEI Quanta 200-ESEM using gaseous secondary electron detector holding the chamber at 3 °C and imaging at 20 kV and 600 Pa.

2.5.9. Transmission electron microscopy (TEM)

Nanoparticle sample was prepared by dispersing the isolated pellet in 5 mL water. A drop of this dispersion was placed on a copper grid and dried under vacuum. Imaging was performed on a transmission electron microscope (CM 200 TEM/Philips/FEI, Inc., Briarcliff Manor, NY, USA) at a voltage of 200 kV having magnification of 0.23 nm after negative staining the sample with uranyl acetate.

2.6. In vitro drug release

In vitro drug release of TMX (15.2 mg) and TMX SNP (~15.2 mg TMX) filled in hard gelatin capsules was evaluated in a USP dissolution apparatus type I (rotating basket) in 900 mL pH 1.2 HCl medium maintained at 37 ± 0.5 °C, at a rotation speed of 100 rpm. Aliquots of 5 mL were withdrawn at intervals of 5, 15, 30, 45 and 60 min and replaced with the same amount of medium. Samples were analyzed by UV spectrophotometry at λ_{max} 275 nm to quantify the amount of TMX released.

2.7. Radiolabeling and biodistribution of TMX in rats by gamma scintigraphy

2.7.1. Radiolabeling of TMX

TMX nanoparticles were prepared by diluting 1 mL SNP (15.2 mg TMX) to 5 mL with water to obtain TMX 380 μg/mL. TMX suspension (380 μg/mL) was prepared by dispersing TMX in an aqueous solution comprising 2% (w/v) sodium carboxymethylcellulose (sodium CMC-7LF). Formulations were radiolabeled with ^{99m}Tc-pertechnetate (^{99m}Tc) by reduction with stannous chloride ($SnCl_2$) (0.1 mg $SnCl_2$ per mCi of ^{99m}Tc) in 0.1N HCl, pH adjusted to 6.5 with 0.1 M sodium bicarbonate, followed by addition of TMX suspension/nanodispersion and incubation at room temperature for 10 min. Labeling efficiency was determined by ascending thin layer chromatography (E-MERCK (India) Ltd., Mumbai). The labeled complex (2–3 μL) was spotted on TLC plates and was developed using acetone as the mobile phase. Radioactivity was measured on a gamma counter (I-125 Gamma Ray Counter IC-4702 – Electronics Corporation of India Ltd.). Stability of the radiolabeled complex was monitored up to 6 h.

2.7.2. Biodistribution of TMX in rats

The Animal Ethics Committee, Bombay Veterinary College, Mumbai (India) had approved the experimental study protocol. Sprague-Dawley rats 2–3 months old with body weight between 200 and 250 g were housed under normal conditions with a 12 h light and dark cycle and were allowed access to food and water ad libitum. Rats were fasted overnight and anesthetized by intraperitoneal injection of a combination of anesthetics, 0.2 mL xylazine injection (Xylaxin, strength – 23.32 mg/mL) and 0.3 mL ketamine hydrochloride injection (Ketmin® 50, strength – 50 mg/mL). ^{99m}Tc radiolabeled formulations, maximum 1 mL (380 μg TMX/mL) were administered by oral gavage to the rats (n = 4). Dynamic images were recorded for 30 min. Static images each of 1 min up to 6 h at intervals of 1 h were captured and processed on eNTEGRA version 2.0318 workstation. The animals were sacrificed by cervical dislocation at the end of 6 h. Organs of interest, namely lungs, liver, spleen, kidneys, heart, stomach, intestines, bone, blood, muscle and tail were removed, washed with normal saline, dried in paper folds and accurately weighed. Radioactivity of the isolated organs and body was quantified using a well-type gamma spectrometer dose calibrator (Capintec-Radioisotope calibrator CRC®-127R of Capintec Inc.). Percent biodistribution of TMX was calculated after decay corrections and expressed as percent injected dose per gram organ.

2.8. Oral bioavailability of TMX in rats

2.8.1. Animal study

The Animal Ethics Committee of the Institute of Chemical Technology, Mumbai (India) had approved the experimental study protocol. In vivo pharmacokinetic studies were carried out in female Sprague–Dawley rats (200–250 g) housed individually under normal conditions, fasted overnight before the experiment with free access to water. Rats were divided into 2 groups, each comprising four rats. TMX nanodispersions were prepared by diluting 1 mL SNP with 4 mL water (3.8 mg TMX/mL) to form nanoparticles of approximately 250 nm size. TMX suspension was prepared by dispersing TMX in a 2% (w/v) aqueous solution of sodium CMC-7LF. Each rat was administered TMX nanodispersion/suspension orally (1 mL). Blood (0.5 mL) was withdrawn from the retro-orbital vein at time intervals of 15, 30, 60, 120, 240, 360 and 1440 min into eppendorf tubes containing 0.1 mL of 4.1% (w/v) EDTA solution. Plasma was separated from the blood samples immediately by centrifugation at 5000 rpm for 5 min. The plasma samples were processed and TMX quantified by HPLC.

2.8.2. HPLC method

A high pressure liquid chromatography method for analysis and separation of TMX from rat plasma was developed. HPLC (Jasco LC 900) system comprised a 100 μl injection loop with Rheodyne injector (model 7725) and Spherisorb® 5 μm ODS2 (4.6 mm × 250 mm) (Waters, USA) analytical column (Ireland). The mobile phase comprised potassium dihydrogen phosphate (pH 3) adjusted with orthophosphoric acid and acetonitrile (30:70, v/v). Chromatography was performed at a flow rate of 1.8 mL/min with UV detection at λ_{max} 275 nm. Data integration was performed using Borwin chromatography software version 1.21. Extraction efficiency was determined by spiking 100, 200, 400, 600 and 800 ng TMX/mL to drug-free plasma (n = 3). Extraction efficiency was calculated by comparing the peak heights of plasma samples with the peak heights of standard TMX solution.

2.8.3. Pharmacokinetic analysis

Pharmacokinetic analysis was performed using the software WinNonlin® Version 4.1 (Pharsight Corporation).

2.9. Data analysis

Results are expressed as mean ± standard deviation and analyzed by GraphPAD Instat Software Program, San Diego, CA. Statistical comparisons were made by analysis of variance (ANOVA) for repeated measures. Differences between values were considered significant when $p < 0.05$.

3. Results and discussion

3.1. Solubility studies

Solubility of TMX and KSR is reported in Fig. 1A and B, respectively. Development of in situ forming drug delivery system requires solvents that are able to form concentrated polymer solutions in order to achieve high drug entrapment and suitable drug release profiles (Kranz et al., 2001). Both TMX and KSR exhibited maximum solubility in Transcutol-P. Hence based on the solubility data, Transcutol-P was selected as the vehicle for development of the SNP.

3.2. Screening of SNP based on nanoparticles formation in situ

Our study is the first to investigate Kollidon® SR for design of a nanoparticulate drug delivery system. Microparticles of Kollidon®

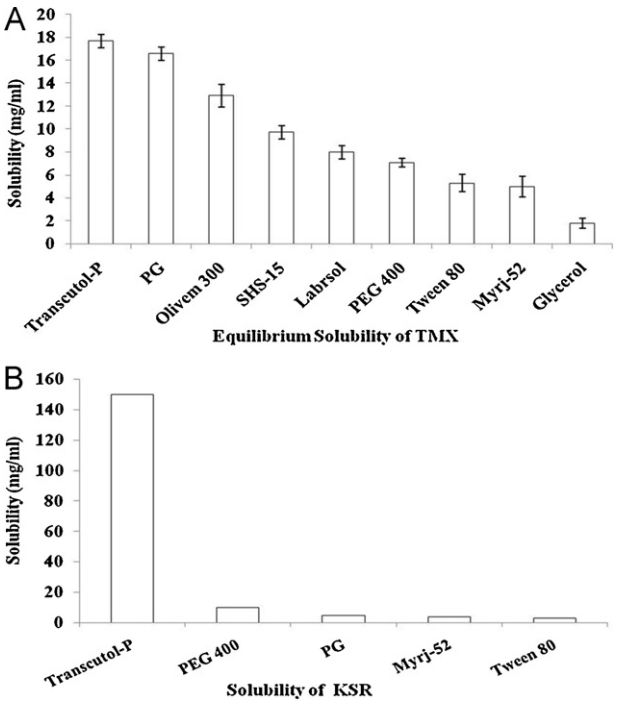

Fig. 1. (A) Equilibrium solubility of TMX in solubilizers and (B) solubility of KSR in solubilizers.

SR for oral delivery of morphine have been reported by Arias et al. (2009a,b).

SNP was initially designed as a simple solution of TMX and KSR in Transcutol-P. Aqueous dilution of the SNP revealed large size, and a heterogeneous size distribution which was visually evident, with fine particles floating and larger particles exhibiting settling.

Inclusion of surfactants enabled a uniform dispersion on dilution. The particle size and entrapment efficiency were influenced by the surfactant. Large PS (>1 μm) and low EE (<30%) were seen with non-ionic surfactants. Anionic surfactant AOT enabled high EE (>80%) due to complexation with cationic TMX. The absence of NH stretching vibrations in the FTIR spectrum confirmed ionic complexation of TMX with AOT (Fig. 6).

Increasing the AOT concentration did not enable reduction in PS. However, surfactant combinations enabled significant decrease in size. Binary surfactant mixtures are a mixture of two surfactants wherein, the properties of the mixture are better than those attainable with the individual components by themselves. The molecular interaction between the two surfactants adsorbed at various interfaces is measured by a parameter molecular interaction parameter (β^{σ}). Molecular interaction parameter (β^{σ}) determines the nature and strength of interaction (i) negative β^{σ} indicates attractive interaction (synergism) and (ii) positive β^{σ} indicates repulsive interactions (antagonism). Further molecular interaction parameter (β^{σ}) quantifies synergism in surface tension reduction efficiency of different charged binary surfactant mixtures. Binary surfactant mixtures are reported to act synergistically to reduce surface tension and enable formation of smaller particles. Molecular interaction parameter is therefore important to enable selection of the optimal binary surfactant combination.

AOT a large surfactant remains largely adsorbed at the interface and forms large cavities in the interfacial layer due to non-uniform distribution of its head group resulting in high surface tension (~40 dyne/cm). Addition of a binary surfactant which could synergistically interact with AOT to fit into the cavities could enable reduction in the surface tension. Synergistic reduction in surface tension with binary surfactants is quantified by the molecular interaction parameter (β^{σ}) which reflects the nature and strength of the interaction. For mixed surfactant films formation at the interface, β^{σ} is calculated using the equations given below (Rosen et al., 1994).

$$\frac{X_1^2 \ln(\alpha C_{12}/X_1 C_1^0)}{(1-X_1)^2 \ln[(1-\alpha)C_{12}/(1-X_1)C_2^0]} = 1$$

$$\beta^{\sigma} = \frac{\ln(\alpha C_{12}/X_1 C_1^0)}{(1-X_1)^2}$$

where α is the mole fraction of surfactant 1 in the total surfactant in the solution phase, $1-\alpha$ is the mole fraction of surfactant 2 in the total surfactant in the solution phase, X_1 is the mole fraction of surfactant 1 in the total surfactant in the mixed monolayer at the surface, C_1^0, C_2^0, C_{12} are the molar concentrations of individual surfactants 1 and 2, respectively, and mixture in solution phase required to produce a given surface tension value and β^{σ} is the molecular interaction parameter for mixed monolayer formation at the aqueous solution–air interface.

While the negative sign of β^{σ} reflects synergistic interaction between surfactants the value β^{σ} indicates the strength of interaction. All the non-ionic surfactants revealed synergistic behavior with AOT. The interaction was in the order PF-68 > Myrj-52 > Tween 80. While the negative sign of β^{σ} reflects synergistic interaction between surfactants the value β^{σ} indicates the strength of interaction. Higher the strength of interaction greater is the reduction in surface tension. A linear relationship ($r^2 = 0.756$) was observed between β^{σ} and surface tension.

Non-ionic surfactant	β^{σ}	Surface tension (dyne)
PF-68	−26.3	32.21
Myrj-52	−8.0	33.54
Tween 80	−5.7	35.41

PF-68 is a linear amphiphilic triblock co-polymer with two equal length hydrophilic poly(ethylene oxide) chains separated by a hydrophobic poly(propylene oxide) block. Tween 80 and Myrj-52 on the other hand, comprise a large polar head and a single short length hydrocarbon chain (Fig. 2).

The linear and flexible nature of PF-68 could facilitate better penetration between the cavities of AOT molecules through formation of a compact loop-tail conformation (Goppert and Muller, 2005). Tween 80 and Myrj-52, although smaller in size, have bulky head groups which hinder interfacial adsorption.

The interaction of binary surfactants and the consequent decrease in surface tension enabled formation of nanosize particles. At 1% and 5% (v/v) the PS with Tween 80 was 238 ± 2.1 nm and 108.9 ± 2.1 nm and with Myrj-52, 208.7 ± 2.5 nm and 116.1 ± 3.2 nm, respectively. PS with PF-68 was larger (1% (w/v) – 395.7 ± 3 nm, 5% (w/v) – 343.9 ± 4.1 nm). A decrease in size was observed with increase in surfactant concentration. Despite maximum decrease in surface tension increase in PS with PF-68 is attributed to aggregation of the small particles, stuck by the emulsifier. Similar observations have been reported by other researchers (Palla and Shah, 2002; Feczko et al., 2008). EE was low (<30%) at high surfactant concentration (5%, w/v). High EE (>80%) and low PS were obtained using a combination of Tween 80 (1%, v/v) and AOT (1.5%, w/v). This surfactant combination was evaluated further.

Altering the drug–polymer (D:P) ratio resulted in no significant change ($p > 0.05$) in EE and PS (Table 1). However extensive settling of the polymer was observed at D:P ratio 1:4. High EE (>80%) and low PS were achieved at D:P ratio 1:1, reflecting a high drug loading of approximately 45% in the KSR nanoparticles.

SNP on dilution generated nanodispersions irrespective of the pH of the aqueous phase. No significant change ($p > 0.05$) in PS and EE was seen in pH 1.2 HCl up to 80 mL, however beyond 80 mL

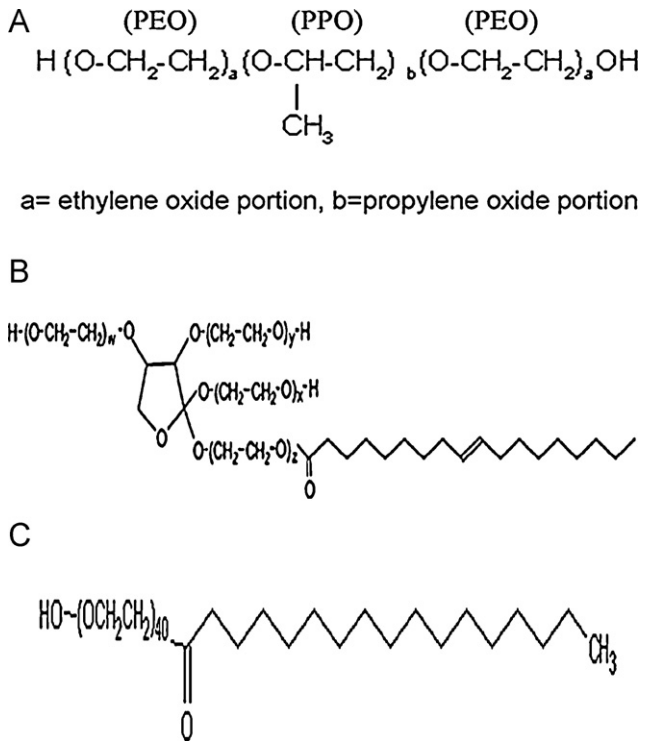

Fig. 2. Structure of (A) Pluronic F 68, (B) Tween 80 and (C) Myrj-52.

Table 1
Effect of TMX:KSR ratio on EE and PS (mean ± S.D.; $n = 4$).

TMX:KSR ratio	EE (%) ± S.D.	PS (nm) ± S.D.	PI
1:1	84.46 ± 1.3	237.70 ± 2.1	0.241
1:2	83.18 ± 3.1	246.65 ± 9.3	0.272
1:3	85.61 ± 2.1	238.60 ± 2.5	0.291
1:4	82.39 ± 4.2	–	–

a decrease in EE and PS was observed (Fig. 3). Increased temperature of dilution medium resulted in a marginal decrease in the nanoparticle size, due to faster solvent diffusion and rapid polymer precipitation. A marginal decrease in both EE and PS was observed over a period of time, similar to that obtained during standard nanoprecipitation (Zhang et al., 2000). TMX SNP under all the experimental conditions when diluted from 4 mL to 80 mL with aqueous media revealed EE between 80 and 87% and PS between 200 and 250 nm, suggesting acceptable performance of the SNP. We do not consider the differences significant to influence in vivo

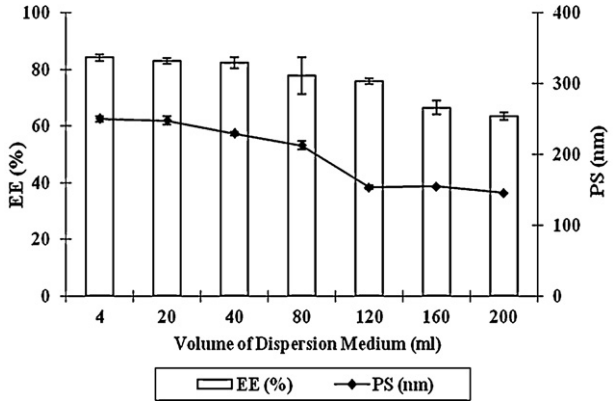

Fig. 3. Effect of volume of dispersion medium on EE and PS of TMX NP.

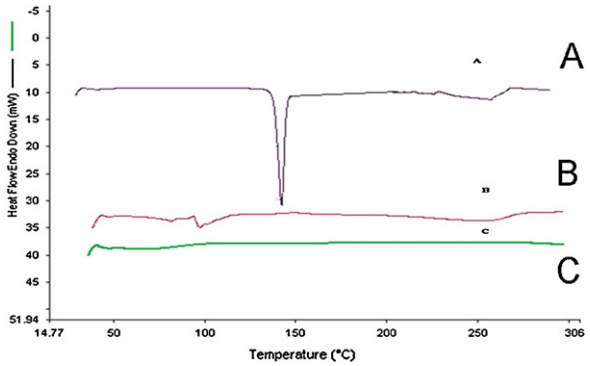

Fig. 4. DSC thermograms of (A) TMX, (B) KSR and (C) TMX NP.

performance if patients are advised to self administer the SNP with a predetermined volume of water. Nevertheless proper patient instructions for administration of the SNP would be imperative.

3.3. DSC

DSC thermogram of TMX revealed a single sharp endothermic peak at 149.5 °C while KSR revealed a melting endotherm at 68.5 °C. The endotherm of TMX totally disappeared in the nanoparticles suggesting conversion of TMX to the amorphous form (Fig. 4).

3.4. XRD

XRD spectra of TMX revealed strong crystalline reflections while KSR exhibited a semi-crystalline nature. The crystallinity of TMX and KSR was maintained in their physical mixture. Absence of sharp reflections of TMX in the nanoparticles suggested conversion of TMX to the amorphous form in the nanoparticles (Fig. 5).

3.5. FTIR

TMX is a quaternary ammonium compound characterized by N—H stretching at 1216 cm^{-1}, aromatic C—C (stretch) at 1630–1582 cm^{-1}, monosubstituted aromatic benzene at 700 cm^{-1} and carbonyl band of citrate at 1728 cm^{-1}. Polymer KSR is a mixture of polyvinylacetate (PVA) and polyvinylpyrrolidone (PVP), wherein PVP is characterized by N—C at 1234 cm^{-1} and PVA by C—O (stretch) at 1117 cm^{-1} and the C=O at 1734 cm^{-1}. Retention of the characteristic peaks of TMX at their respective wave numbers in the nanoparticles indicates the absence of chemical or ionic interaction between TMX and KSR (Fig. 6).

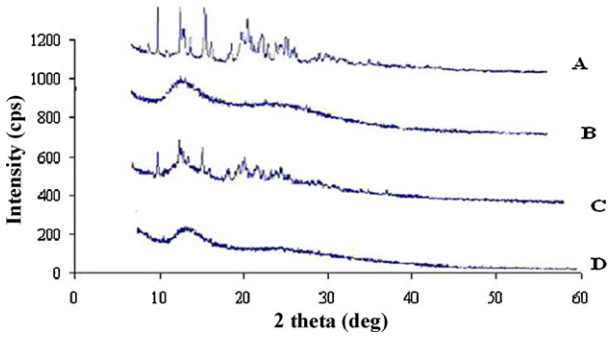

Fig. 5. XRD spectra of (A) TMX, (B) KSR, (C) TMX-KSR physical mixture and (D) TMX NP.

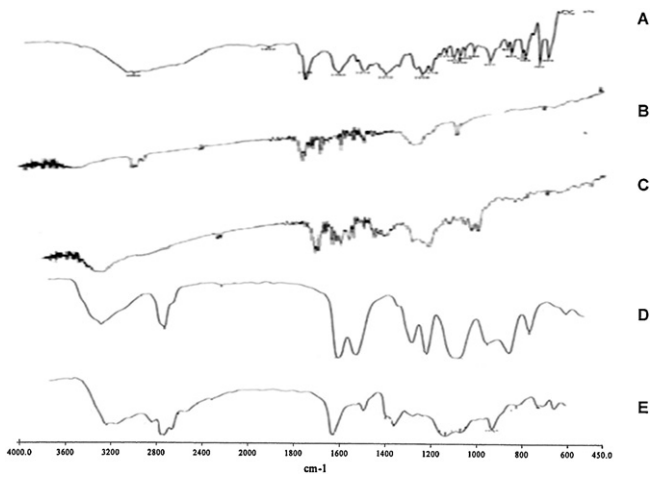

Fig. 6. FTIR spectra of (A) TMX, (B) AOT, (C) TMX-AOT ionic complex, (D) KSR and (E) TMX NP.

3.6. FTIR microscopy and imaging

FTIR microscopy is a powerful and comprehensive technique which combines image analysis of microscopy and chemical analysis of FTIR spectroscopy to enhance imaging sensitivity. The spectral change information can be related to the microstructure of the sample confirming its existence and content (Coutts-Lendon et al., 2003).

Fig. 7A depicts the FTIR image of TMX nanoparticles, while the inset indicates the points at which the spectra were extracted. The overlay of spectra of the 5 points (Fig. 7B) reflects homogeneity and uniform distribution of TMX in the nanoparticles. Homogeneous distribution and conformation of lysozyme in a biodegradable polymer matrix has been demonstrated using infrared microscopy (Weert et al., 2000).

3.7. ESEM

ESEM is a straightforward analysis technique with the ability for dynamic imaging, correlated to relative humidity of real atmospheric condition. It enables visualization and provides supportive information of the existence of nanoparticles in the suspension state (Erickson et al., 2005; Laskin et al., 2006). Low contrast ESEM images are due to movement of nanoparticles in the liquid state and lack of conductive coating during ESEM operation (Bogner et al., 2005; Pongpeerapat et al., 2008). ESEM image of TMX nanoparticle with AOT revealed formation of agglomerates (Fig. 8A) while TMX nanoparticle with AOT and Tween 80 revealed spherical nanosize particles (≈300 nm) (Fig. 8B). Nanoparticle size measurements by ESEM correlated well with photon correlation spectroscopy measurements.

3.8. TEM

TEM image of TMX nanoparticles revealed spherical morphology and nanosize which correlated well with the photon correlation spectroscopy measurements (Fig. 9).

3.9. In vitro drug release

TMX revealed slow release compared to the SNP. Nanodispersions generated in situ by the dilution of the SNP revealed 100% drug release at the end of 1 h (Fig. 10). Rapid release of TMX from nanodispersions suggests that TMX was localized at the nanoparticles surface, indicated by the positive zeta potential value (+9.83 mV).

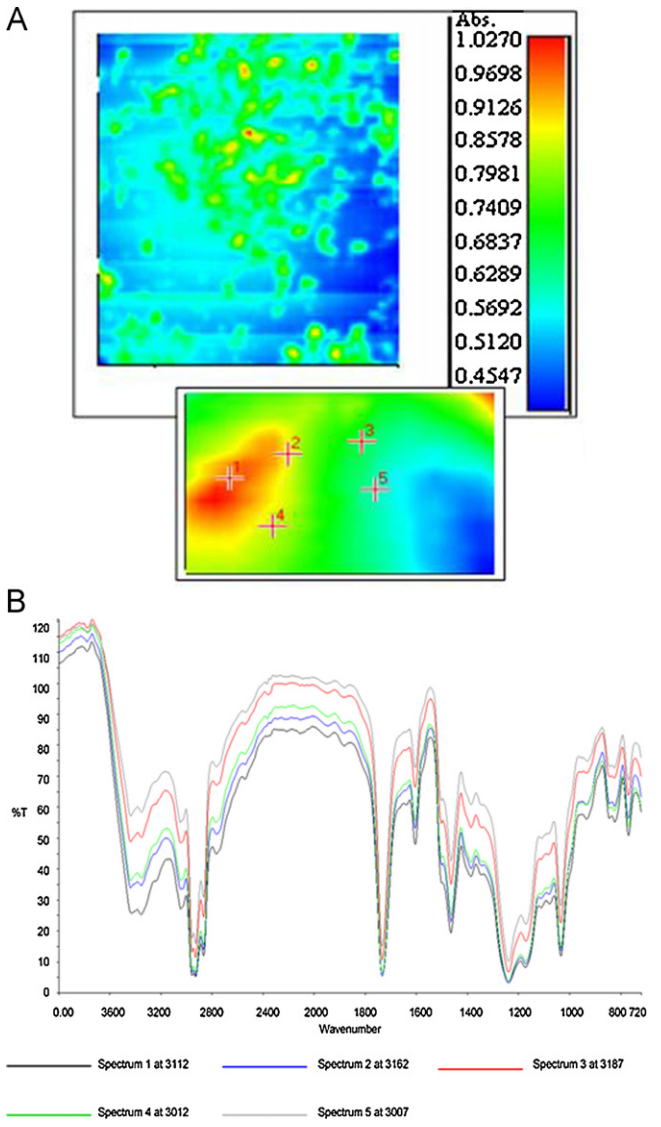

Fig. 7. FTIR imaging of (A) infrared image of TMX NP (color on scale bar represents different integrated absorbance values) and (B) overlay of TMX NP spectra. (For interpretation of the references to color in this figure legend, the reader is referred to the web version of this article.)

TMX release was characterized by four basic models zero-order kinetic model, first-order kinetic model, Higuchi kinetic model and Korsmeyer–Peppas model. In Korsmeyer–Peppas equation the value of diffusion release exponent n dictates drug release mechanism. Drug release in zero order, non-Fickian diffusion and Fickian diffusion is represented by $0.89 < n < 1$, $0.45 < n < 0.89$, and $n = 0.45$, respectively (Merchant et al., 2006). The value of n for release from TMX nanoparticles was 0.91, with $r^2 = 0.991$ for the zero order kinetic model indicating zero order drug release.

3.10. Radiolabeling and biodistribution of TMX nanoparticles in rats

^{99m}Tc labeled complex of TMX nanoparticles and TMX suspension revealed an average radiolabeling binding efficiency of 90.68% and 87.22%, respectively at the end of 6 h at 28 °C. The stability of ^{99m}Tc labeled complex for a period of 6 h indicated their use for biodistribution studies. Absence of ^{99m}Tc labeled complex in the thyroid confirmed the in vivo stability of the radiolabeled complex.

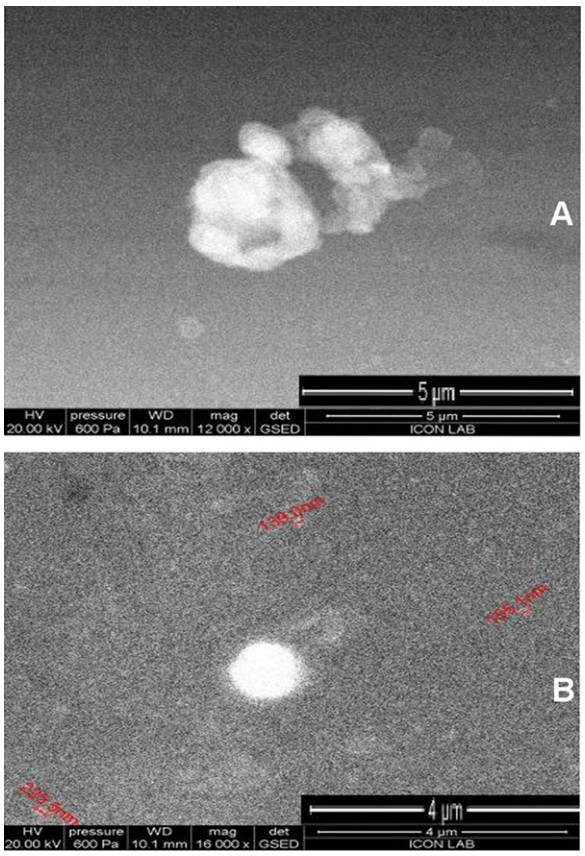

Fig. 8. ESEM image of (A) TMX NP with AOT and (B) TMX NP with AOT and Tween 80 at 16,000× magnification.

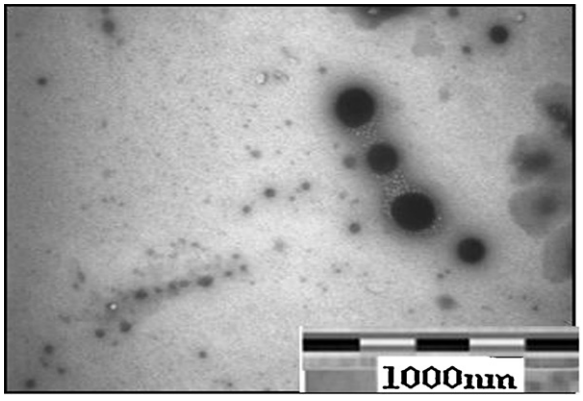

Fig. 9. TEM image of TMX NP with AOT and Tween 80.

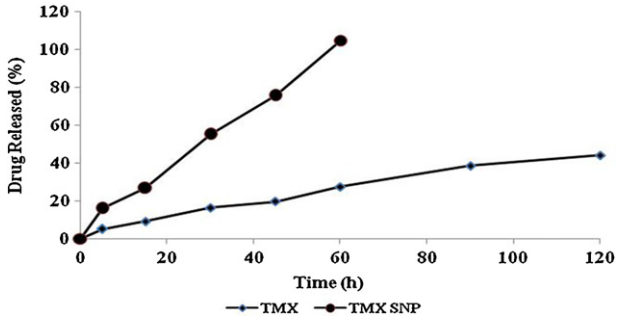

Fig. 10. In vitro release profile of TMX and TMX SNP.

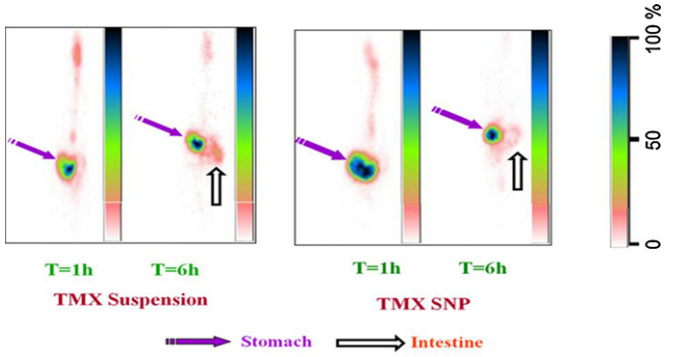

Fig. 11. Gamma scintigraphy images of biodistribution profile at 1 h and 6 h post oral administration for ^{99m}Tc-labeled TMX suspension and TMX SNP.

^{99m}Tc-labeled TMX nanoparticles on oral administration propagated from the oesophagus to the stomach and intestines (small and large) with time. At 6 h post ingestion majority of the radioactivity was observed in the stomach with low amounts in the intestine. The general distribution in the organs of interest namely kidneys, liver, spleen, heart and lungs was <1% and was not statistically significant ($p > 0.05$) (Figs. 11 and 12) (Chen et al., 2009). Presence of high activity in stomach can be due to presence of sex steroids such as estrogen and androgen. Similar observations have been reported by other researchers (Kon, 1983; Winborn et al., 1987; Ciocca and Vargas, 1995; Biber Muftuler et al., 2008).

3.11. Oral bioavailability of TMX in rats

3.11.1. HPLC method for detection of TMX in plasma

A simple, rapid, precise and accurate HPLC method was developed for evaluation of TMX in rat plasma. The method was linear in the concentration range of 40–1000 ng/mL. Good recovery was obtained at concentrations 100, 200, 400, 600 and 800 ng/mL with an extraction efficiency of 84.51 ± 3.1% for TMX from plasma.

3.11.2. Bioavailability of TMX nanoparticles in rats

TMX is reported to exhibit poor bioavailability following oral administration. Orally administered TMX nanoparticles enabling rapid dissolution of TMX, and direct lymphatic uptake through the GALT and MALT were expected to significantly enhance the bioavailability (Florence, 1997). Fig. 13 and Table 2 confirm the enhanced bioavailability of TMX nanoparticles with a relative bioavailability of 165.61% compared to TMX. A significant enhancement in C_{max} is also observed. The k_{el} and $t_{1/2}$ of TMX nanoparticles and TMX were comparable (15–16 h) and analogous with reported data on TMX (Jain et al., 2011). Although no significant absorption

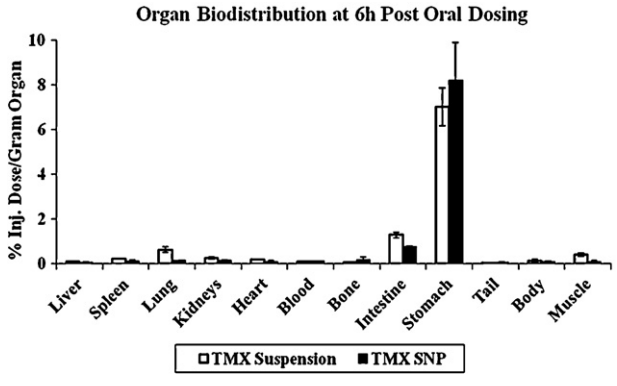

Fig. 12. Comparative biodistribution profile of ^{99m}Tc-labeled TMX suspension and TMX SNP 6 h post oral administration.

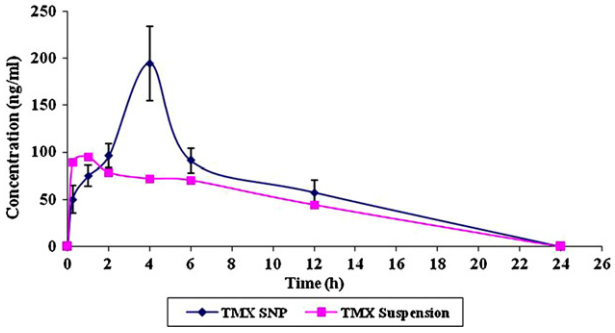

Fig. 13. Mean plasma concentration–time curve of TMX after oral administration of TMX SNP and suspension in rat ($n = 4$).

Table 2
Pharmacokinetic parameters of TMX suspension and TMX SNP after oral administration in rats (mean ± S.D.; $n = 4$).

Parameters	TMX suspension	TMX SNP
C_{max} (h ng/mL)	95	195
T_{max} (h)	1	4
AUC_{0-24} (h ng/mL)	1354.96	2072.14
$AUC_{0-infinity}$ (h ng/mL)	2056.20	3405.10
K_{el} (h^{-1})	0.043	0.045
$T_{1/2}$ (h)	16.00	15.35
Cl (mL/h)	1848.06	1115.79
Fr (%)	–	165.61

of TMX was evident in the gamma scintigraphy studies (Chen et al., 2009), the pharmacokinetic study of TMX in rats revealed high TMX bioavailability. Recently high bioavailability and improved in vivo antitumor efficacy following oral administration of PLGA TMX nanoparticles has been reported (Jain et al., 2011). Since breast cancer generally metastases through the lymph, oral administration of SNP would enable absorption of TMX nanoparticles through M-cells to the lymph (Florence, 1997) and hence provide improved benefits in the therapy of breast cancer (Andrianov and Payne, 1998; Clark et al., 2001; Hussain et al., 2001; Coppi and Iannuccelli, 2009).

4. Conclusions

Polymeric nanoparticles of TMX by enabling high bioavailability and possible lymphatic uptake could provide significant enhanced therapeutic benefits in breast cancer metastases. Nevertheless a significant limitation in their clinical translation is the lack of technology for scale up and the high cost involved therein. An important advantage of the SNP is the design of a simple monophasic system to provide nanoparticles with >80% drug entrapped. SNP of TMX could provide a practical and technologically feasible nano delivery system with significantly improved efficiency in breast cancer therapy. We further plan to evaluate the SNP of TMX in vivo in breast cancer model.

Nanoprecipitation under defined conditions has shown to reproducibly form nanoparticles, nevertheless these nanoparticles need to be isolated, purified and freeze dried to permit applications. In comparison, our new approach through design of SNP, optimized judiciously using a binary surfactant composition provides both the biological advantage of polymeric nanoparticles with high entrapment efficiency and probable lymphatic uptake, coupled with a technological superiority.

Acknowledgments

Sonali V. Kapse acknowledges University Grant Commission (UGC), Government of India for providing Senior Research Fellowship. Authors wish to acknowledge Tata Institute of Fundamental Research (TIFR) (Mumbai-India) for XRD study and Perkin Elmer Pvt. Ltd (Mumbai, India) for FTIR microscopy and Imaging.

References

Allen, T.M., Cullis, P.R., 2004. Drug delivery systems: entering the mainstream. Science 303, 1818–1822.
Andrianov, A.K., Payne, L.G., 1998. Polymeric carriers for oral uptake of microparticulates. Adv. Drug Deliv. Rev. 34, 155–170.
Arias, J.L., Gallo, A.G., Delgado, Á.V., Ruiz, M.A., 2009a. Kollidon® SR colloidal particles as vehicles for oral morphine delivery in pain treatment. Colloids and Surfaces B 70, 207–212.
Arias, J.L., Gallo, A.G., Delgado, Á.V., Gallardo, V., 2009b. Study of the stability of Kollidon® SR suspensions for pharmaceutical applications. Colloid Surface A 338, 107–113.
Biber Muftuler, F.Z., Unak, P., Teksoz, S., Acar, C., Yolcular, S., Yurekli, Y., 2008. ^{131}I labeling of tamoxifen and biodistribution studies in rats. Appl. Radiat. Isot. 66, 178–187.
Bogner, A., Thollet, G., Basset, D., Jouneau, P.H., Gauthier, C., 2005. Wet STEM: a new development in environmental SEM for imaging nano-objects included in a liquid phase. Ultramicroscopy 104, 290–301.
Buckley, M.M., Goa, K.L., 1989. Tamoxifen. A reappraisal of its pharmacodynamic and pharmacokinetic properties and therapeutic use. Drugs 37, 451–490.
Chawla, J.S., Amiji, M.M., 2002. Biodegradable poly(caprolactone) nanoparticles for tumor targeted delivery of tamoxifen. Int. J. Pharm. 249, 127–138.
Ciocca, D.R., Vargas, L.M., 1995. Estrogen receptors in human nontarget tissues: biological and clinical implications. Endocrine Rev. 16, 35–62.
Clark, M.A., Jepson, M.A., Hirst, B.H., 2001. Exploiting M cells for drug and vaccine delivery. Adv. Drug Deliv. Rev. 50, 81–106.
Coppi, G., Iannuccelli, V., 2009. Alginate/chitosan microparticles for tamoxifen delivery to the lymphatic system. Int. J. Pharm. 367, 127–132.
Coutts-Lendon, C.A., Wright, N.A., Mieso, E.V., Koenig, J.L., 2003. The use of FT-IR imaging as an analytical tool for the characterization of drug delivery systems. J. Control. Release 93, 223–248.
Couvreur, P., Vauthier, C., 2006. Nanotechnology: intelligent design to treat complex disease. Pharm. Res. 23, 1417–1450.
Dong, W.Y., Körber, M., Esguerra, V.L., Bodmeier, R., 2006. Stability of poly(D,L-lactide-co-glycolide) and leuprolide acetate in *in situ* forming drug delivery systems. J. Control. Release 115, 158–167.
Erickson, K.L., Bostrom, T.E., Frost, R.L., 2005. A study of structural memory effects in synthetic hydrotalcites using environmental SEM. Mater. Lett. 59, 226–229.
Farokhzad, O.C., Cheng, J., Teply, B.A., Sherifi, I., Jon, S., Kantoff, P.W., Richie, J.P., Langer, R., 2006. Targeted nanoparticle-aptamer bioconjugates for cancer chemotherapy *in vivo*. PNAS 103, 6315–6320.
Fasinu, P., Pillay, V., Ndesendo, V.M.K., du Toit, L.C., Choonara, Y.E., 2011. Diverse approaches for the enhancement of oral drug bioavailability. Biopharm. Drug Dispos. 32, 185–209.
Feczko, T., Toth, J., Gyenis, J., 2008. Comparison of the preparation of PLGA–BSA nano- and microparticles by PVA, poloxamer and PVP. Colloid Surface A 319, 188–195.
Florence, A.T., 1997. The oral absorption of micro- and nanoparticulates: neither exceptional nor unusual. Pharm. Res. 14, 259–266.
Goppert, T.M., Muller, R.H., 2005. Protein adsorption patterns on poloxamer- and poloxamine-stabilized solid lipid nanoparticles (SLN). Eur. J. Pharm. Biopharm. 60, 361–372.
Hussain, N., Jaitley, V., Florence, A.T., 2001. Recent advances in the understanding of uptake of microparticulate across the gastrointestinal lymphatics. Adv. Drug Deliv. Rev. 50, 107–142.
Jain, R., 2000. The manufacturing techniques of various drug loaded biodegradable poly(lactide-co-glycolide) (PLGA) devices. Biomaterials 21, 2475–2490.
Jain, A.K., Swarnakar, N.K., Godugu, C., Singh, R.P., Jain, S., 2011. The effect of the oral administration of polymeric nanoparticles on the efficacy and toxicity of tamoxifen. Biomaterials 32, 503–515.
Kon, O.L., 1983. An antiestrogen binding protein in human tissues. J. Biol. Chem. 258, 3173–3177.
Körber, M., Bodmeier, R., 2008. Development of an *in situ* forming PLGA drug delivery system I. Characterization of a non-aqueous protein precipitation. Eur. J. Pharm. Sci. 35, 283–292.
Kranz, H., Bodmeier, R., 2007. A novel *in situ* forming drug delivery system for controlled parenteral drug delivery. Int. J. Pharm. 332, 107–114.
Kranz, H., Brazeau, G.A., Napaporn, J., Martin, R.L., Millard, W., Bodmeier, R., 2001. Myotoxicity studies of injectable biodegradable *in situ* forming drug delivery systems. Int. J. Pharm. 212, 11–18.
Laskin, A., Cowin, J.P., Iedema, M.J., 2006. Analysis of individual environmental particles using modern methods of electron microscopy and X-ray microanalysis. J. Electron Microsc. Relat. Phenom. 150, 260–274.

Li, J., Chen, F., Hu, C., He, L., Yan, K., Zhou, L., Pan, W., 2008. Optimized preparation of *in situ* forming microparticles for the parenteral delivery of vinpocetine. Chem. Pharm. Bull. 56, 796–801.

Luan, X., Bodmeier, R., 2006a. *In situ* forming microparticle system for controlled delivery of leuprolide acetate: influence of the formulation and processing parameters. Eur. J. Pharm. Sci. 27, 143–149.

Luan, X., Bodmeier, R., 2006b. Influence of the poly(lactide-co-glycolide) type on the leuprolide release from *in situ* forming microparticle systems. J. Control. Release 110, 266–272.

McVie, J.G., Simonetti, G.P., Stevenson, D., Brigss, R.J., Guelen, P.J., de Vos, D., 1986. The bioavailability of Tamoplex (Tamoxifen). Part 1. A pilot study. Methods Find. Exp. Clin. Pharmacol. 8, 505–512.

Chen, M.-C., Wong, H.-S., Lin, K.-J., Chen, H.-L., Wey, S.-P., Sonaje, K., Lin, Y.-H., Chu, C.-Y., Sung, H.-W., 2009. The characteristics, biodistribution and bioavailability of a chitosan-based nanoparticulate system for the oral delivery of heparin. Biomaterials 30, 6629–6637.

Merchant, H.A., Shoaib, H.M., Tazeen, J., Yousuf, R.I., 2006. Once-daily tablet formulation and in vitro release evaluation of cefpodoxime using hydroxypropyl methylcellulose: a technical note. AAPS PharmSci. Tech. 7, E1–E6.

Palla, B.J., Shah, D.O., 2002. Stabilization of high ionic strength slurries using surfactant mixtures: molecular factors that determine optimal stability. J. Colloid Interf. Sci. 202, 143–152.

Panyam, J., Labhasetwar, V., 2003. Biodegradable nanoparticles for drug and gene delivery to cells and tissue. Adv. Drug Deliv. Rev. 55, 329–347.

Pongpeerapat, A., Wanawongthai, C., Tozuka, Y., Moribe, K., Yamamotoa, K., 2008. Formation mechanism of colloidal nanoparticles obtained from probucol/PVP/SDS ternary ground mixture. Int. J. Pharm. 352, 309–316.

Rosen, M.J., Gao, T., Nakatsuji, Y., Masuyama, A., 1994. Synergism in binary mixtures of surfactants 12. Mixtures containing surfactants with two hydrophilic and two or three hydrophobic groups. Colloid Surface A 88, 1–11.

Soppimath, K.S., Aminabhavi, T.M., Kulkarni, A.R., Rudzinsk, W.E., 2001. Biodegradable polymeric nanoparticles as drug delivery devices. J. Control. Release 70, 1–20.

Tukker, J.J.,.Blankenstein, M.A., Nortier, J.W., 1986. Comparison of bioavailability in man of tamoxifen after oral and rectal administration. J. Pharm. Pharmacol. 38, 888–892.

Weert, M., Hof, R., Weerd, J., Heeren, R.M.A., Posthuma, G., Hennink, W.E., Crommelin, D.J.A., 2000. Lysozyme distribution and conformation in a biodegradable polymer matrix as determined by FTIR techniques. J. Control. Release 68, 31–40.

Winborn, W.B., Sheridan, P.J., McGill, H.C., 1987. Sex steroids in the stomach, liver, pancrease, and gastrointestinal tract of the baboon. Gastroenterology 92, 23–32.

Zhang, Q., Yie, G., Li, Y., Yang, Q., Nagai, T., 2000. Studies on the cyclosporin A loaded stearic acid nanoparticles. Int. J. Pharm. 200, 153–159.